Acta Crystallographica Section A
Foundations and Advances
ISSN 2053-2733

Received 10 June 2014
Accepted 2 November 2014

Symmetry groups associated with tilings on a flat torus

Mark L. Loyola, Ma. Louise Antonette N. De Las Peñas,* Grace M. Estrada and Eko Budi Santoso

Mathematics Department, Ateneo de Manila University, Katipunan Avenue, Loyola Heights, Quezon City, Metro Manila 1108, Philippines. Correspondence e-mail: mdelaspenas@ateneo.edu

This work investigates symmetry and color symmetry properties of Kepler, Heesch and Laves tilings embedded on a flat torus and their geometric realizations as tilings on a round torus in Euclidean 3-space. The symmetry group of the tiling on the round torus is determined by analyzing relevant symmetries of the planar tiling that are transformed to axial symmetries of the three-dimensional tiling. The focus on studying tilings on a round torus is motivated by applications in the geometric modeling of nanotori and the determination of their symmetry groups.

1. Introduction

Following the discovery of carbon nanotubes by Sumio Iijima (1991), much interest has been focused on the study of other possible forms of carbon. These forms are essentially structural variations on the bonding arrangements of carbon atoms. When a single-wall carbon nanotube is bent and its opposite ends are connected, one obtains a toroidal structure called a *carbon nanotorus*. A carbon nanotorus can be described as a network of carbon hexagons arranged compactly on a round torus surface (the surface of a doughnut). The successful synthesis of stable carbon nanotori from chemically reacted carbon nanotubes was reported in Martel *et al.* (1999) and Sano *et al.* (2001).

The attention researchers have paid in studying carbon nanotori is in part driven by these nanostructures' promising technological applications. These applications depend on the properties nanotori possess or are predicted to exhibit. Calculations show that carbon nanotori possess a wide range of structural (Liu *et al.*, 2001), electronic (Haddon, 1997; Oh *et al.*, 2000), optical and vibrational (Beuerle *et al.*, 2011), and magnetic properties (Liu *et al.*, 2001; Liu & Xu, 2008).

Deriving the properties of a carbon nanotorus requires a geometric model to which calculations will be applied. These calculations often factor in the symmetry structure of the nanotorus. Some properties can, in fact, be described directly through the language of symmetry or any of its generalizations. Dienes & Thomas (2011), for instance, used the notion of modular symmetries to discuss spectral equivalences among physically distinct nanotori.

Motivated by the geometric modeling of nanotori and the determination of their symmetry groups, we build on the works of Senechal (1988) and Sullivan (2011) to study the geometry and symmetry structures of tilings on a flat torus and their realizations as tilings on a round torus in the Euclidean 3-space $\mathbb{E}^3$. Starting with a Kepler, Heesch or Laves tiling $\mathbb{T}$, which are tilings of the plane with transitivity properties (Appendix *A*), we obtain *via* an orbit-space construction a tiling $\mathbb{T}^*$ on a flat torus. A tiling on a round torus is obtained subsequently by projecting $\mathbb{T}^*$ to $\mathbb{E}^3$ *via* a map that generalizes the conformal map provided in Sullivan (2011).

This work uses tiling by hexagons embedded on a round torus to model a carbon nanotorus. Carbon atoms are represented by the vertices of the tiling while atomic bonds are represented by the edges [a related work is found in Staic & Petrescu-Nita (2013) where torus-embedded Cayley hypergraphs were used to model carbon nanotori]. A theoretical nanotorus with non-hexagonal symmetries such as a C_4C_8 nanotorus (Ashrafi & Shabani, 2009) will be obtained from a monolayer modeled by a Kepler tiling. When the nanotorus is obtained from a monolayer made up of different types of atoms, such as a boron nitride nanotorus (Loh & Baillargeat, 2013), we introduce colors on the vertices of the tiling to distinguish one type of atom from another.

The approach of determining the symmetry group of a tiling on a round torus or a nanotorus involves analyzing and identifying symmetries of $\mathbb{T}$ that are transformed to *axial symmetries*. When the vertices, edges or faces of $\mathbb{T}$ are colored, we analyze the color-fixing symmetries of $\mathbb{T}$ that are transformed to axial symmetries of the corresponding colored tiling on the round torus. We use as a starting point in the analysis the plane crystallographic group type of the symmetry group of the uncolored tiling or the color-fixing group of the colored tiling, and from this two-dimensional setting, we arrive at results pertaining to the symmetry group of a three-dimensional geometric structure. This approach lends a convenient method to determine symmetries of a structure by looking at symmetries of an associated structure in a space of lower dimension. It is analogous to the approach used by De Las Peñas *et al.* (2014) to determine the line-group type of the symmetry group of a single-wall nanotube. Another advantage of the approach is that it allows the relevant non-rigid motions

of a nanotorus considered in the literature (Bovin *et al.*, 2001; Arezoomand & Taeri, 2009; Zhao *et al.*, 2012) to be derived and characterized as four-dimensional symmetries. This offers a rigorous treatment of these motions as Euclidean symmetries.

We begin the discussion by first introducing the mathematical formalism needed to understand tilings on a flat torus and their symmetry groups in the next section.

2. Tiling $\mathbb{T}^*$ on a flat torus

Let $\mathbb{T}$ be a Kepler, Heesch or Laves tiling in the Euclidean plane $\mathbb{E}^2$. The symmetry group G of $\mathbb{T}$ is a plane crystallographic group with translation subgroup $T(G)$ generated by two linearly independent translations x and y. G acts transitively on the set X of vertices, edges or faces of a Kepler, Heesch or Laves tiling $\mathbb{T}$, respectively. Let L be the subgroup of $T(G)$ generated by $x^{m_1}y^{m_2}$ and $x^{n_1}y^{n_2}$, where $m_1, m_2, n_1, n_2 \in \mathbb{Z}$ and $m_1n_2 - m_2n_1 \neq 0$. L acts freely on $\mathbb{E}^2$ and defines the *orbit space* $\mathbb{E}^2/L = \{Lu : u \in \mathbb{E}^2\}$ called a *flat torus*. This space is the collection of all orbits of points in $\mathbb{E}^2$ under L. More specifically, a point $v \in \mathbb{E}^2$ belongs to the orbit Lu of $u \in \mathbb{E}^2$ if and only if $v = lu$ for some $l \in L$.

The Kepler, Heesch or Laves tiling $\mathbb{T}$ gives rise to the tiling $\mathbb{T}^* = \mathbb{T}/L$ on the flat torus $\mathbb{E}^2/L$. Since a flat torus is a quotient space of $\mathbb{E}^2$, it is endowed with a metric inherited from $\mathbb{E}^2$ (McMullen & Schulte, 2002). With respect to this metric, the group G^* consisting of all distance-preserving bijective transformations of $\mathbb{E}^2/L$ that leave $\mathbb{T}^*$ invariant is isomorphic to $N_G(L)/L$, where $N_G(L) = \{g \in G : gLg^{-1} = L\}$ is the normalizer of L in G (McMullen & Schulte, 2002; Senechal, 1988). It acts on $X/L = \{L\chi : \chi \in X\}$, the set of (respectively) vertices, edges or faces of $\mathbb{T}^*$, by left multiplication. More precisely, if $Lg \in N_G(L)/L$ and $L\chi \in X/L$, then $Lg \cdot L\chi = L(g\chi) \in X/L$.

It is routine to show that $N_G(L)$ is a translation-equivalent subgroup of G. That is, $T(N_G(L)) = T(G)$. Note that $N_G(L)$ is also a plane crystallographic group and is an extension of $T(G)$ by its point group $P(N_G(L))$. As a special case, when $N_G(L)$ is a symmorphic group or a split extension of $T(G)$ by $P(N_G(L))$, $G^* \cong (T(G)/L) \rtimes P(N_G(L))$.

The following theorem is helpful in characterizing the structure of G^*.

Theorem 1. Let $T(G) = \langle x, y\rangle$ be the translation subgroup of a plane crystallographic group G and let $L = \langle x^{m_1}y^{m_2}, x^{n_1}y^{n_2}\rangle$ be a subgroup of $T(G)$, where $m_1, m_2, n_1, n_2 \in \mathbb{Z}$ and $m_1n_2 - m_2n_1 \neq 0$. Then $T(G)/L \cong C_d \times C_{|m_1n_2-m_2n_1|/d}$, where $d = \gcd(m_1, m_2, n_1, n_2)$.

Proof. Since $T(G) = \langle x, y\rangle$ is a $\mathbb{Z}$-module with basis x and y, we can express $L = \langle x^{m_1}y^{m_2}, x^{n_1}y^{n_2}\rangle$ in matrix form as

$$\mathbf{L} = \begin{bmatrix} m_1 & n_1 \\ m_2 & n_2 \end{bmatrix}.$$

A useful result (Sims, 1994) states that $T(G)/L$ is isomorphic to the direct product $C_{\delta_1} \times C_{\delta_2}$ of finite cyclic groups, where δ_1 and δ_2 are the diagonal entries in the Smith normal form of the matrix $\mathbf{L}$. Computation using determinantal divisors (Adkins & Weintraub, 1999) yields $\delta_1 = d$ and $\delta_2 = |m_1n_2 - m_2n_1|/d$, where d is the greatest common divisor of m_1, m_2, n_1 and n_2. □

3. Colorings of $\mathbb{T}^*$

Consider the set X of vertices, edges or faces of a Kepler, Heesch or Laves tiling $\mathbb{T}$, respectively. If $C = \{c_1, c_2, \ldots, c_k\}$ is a set of k colors, we define a *k-coloring* of $\mathbb{T}$ to be a surjective function $f : X \to C$, which assigns to each $\chi \in X$ a color $f(\chi)$ in C. The coloring f determines a partition $\mathcal{P} = \{f^{-1}(c_i) : c_i \in C\}$ of X, where $f^{-1}(c_i)$ is assigned the color c_i.

Let H be the subgroup of G which consists of symmetries of $\mathbb{T}$ that effect a permutation of the colors in C. Then $h \in H$ if for every $c_i \in C$, there is a $c_j \in C$ such that $h(f^{-1}(c_i)) = f^{-1}(c_j)$. This defines an action of H on C where we define $hc_i := c_j$ if and only if $h(f^{-1}(c_i)) = f^{-1}(c_j)$. The group H is called the *color group* and the elements of H are referred to as the *color symmetries* of the given coloring of $\mathbb{T}$. The group K of symmetries in H that fix the colors is called the *color-fixing group* associated with the coloring. If $H = G$, then the coloring of $\mathbb{T}$ is called a *perfect coloring*.

To obtain a coloring of the tiling $\mathbb{T}^*$ on the flat torus $\mathbb{E}^2/L$ from the coloring of the tiling $\mathbb{T}$ in the plane and conversely, L must be a subgroup of K to ensure that no two distinct colors overlap in the flat torus. Given a k-coloring $f : X \to C$ of $\mathbb{T}$, we obtain a k-coloring $f^* : X/L \to C$ of $\mathbb{T}^*$ defined by $f^*(L\chi) := f(\chi)$, $L\chi \in X/L$. On the other hand, given a k-coloring $f^* : X/L \to C$ of $\mathbb{T}^*$, we obtain a k-coloring $f : X \to C$ of $\mathbb{T}$ defined by $f(\chi) := f^*(L\chi)$, $\chi \in X$.

The color group and color-fixing group of the colorings discussed above are described in the next theorem.

Theorem 2. Let $f : X \to C$ define a coloring of $\mathbb{T}$ with color group H and color-fixing group K. Then the color group H^* and color-fixing group K^* of the coloring f^* of $\mathbb{T}^*$ are given by $H^* = N_H(L)/L$ and $K^* = N_K(L)/L$, respectively. Conversely, if $f^* : X/L \to C$ is a coloring of $\mathbb{T}^*$ with color group $H^* = H'/L$ and color-fixing group $K^* = K'/L$, where $H', K' \leq N_G(L)$, then the color group H and color-fixing group K of the coloring f satisfy $H' \leq H$ and $K' \leq K$, respectively.

Proof. Let $H^* \leq G^* = N_G(L)/L$ be the color group of f^* and let $Lh \in H^*$, $h \in N_G(L)$. Then for every $c_i \in C$, there is a $c_j \in C$ such that $(Lh)((f^*)^{-1}(c_i)) = (f^*)^{-1}(c_j)$. This implies that $(Lh)c_i = c_j$ and $hc_i = c_j$. Thus, $h \in H$ and $Lh \in N_H(L)/L$. For the reverse direction, let $Lh \in N_H(L)/L$, $h \in H$. Then for every $c_i \in C$, there is a $c_j \in C$ such that $hc_i = c_j$. Since $L \leq K$, $(Lh)c_i = c_j$. This implies that $(Lh)((f^*)^{-1}(c_i)) = (f^*)^{-1}(c_j)$. Thus, $Lh \in H^*$. Analogously, if $K^* \leq H^*$ denotes the color-fixing group of f^*, then $Lk \in K^*$ if and only if $Lk \in N_K(L)/L$.

Suppose now that $h \in H'$. Then $Lh \in H^*$. It follows that for every $c_i \in C$, there is a $c_j \in C$ such that $(Lh)((f^*)^{-1}(c_i)) = (f^*)^{-1}(c_j)$ or $(Lh)c_i = c_j$. Consequently, $hc_i = c_j$. Thus $h \in H$. Next, let $k \in K'$ so that $Lk \in K^*$. Hence, $(Lk)((f^*)^{-1}(c_i)) = (f^*)^{-1}(c_i)$ for every $c_i \in C$, and thus, $kc_i = c_i$. Therefore, $k \in K$. □

The following result whose proof follows immediately from Theorem 2 gives a necessary and sufficient condition for a perfect coloring of $\mathbb{T}^*$.

Corollary 1. A coloring $f^* : X/L \to C$ of $\mathbb{T}^*$ is perfect if and only if the color group H of the coloring $f : X \to C$ satisfies $N_G(L) \leq H$.

To illustrate the above results, we consider a tiling by regular hexagons $\mathbb{H} = (6^3)$, a Kepler tiling with symmetry group $G = \langle x, y, a, b\rangle \cong p6mm$ (IUCr notation) generated by the translations x, y with vectors separated by an angle of $2\pi/3$ radians, the sixfold (counterclockwise) rotation a about O, and the reflection b in the axis through O in the direction of x (Fig. 1*a*). Consider the vertex 4-coloring of $\mathbb{H}$ shown in Fig. 1(*b*). The coloring has color group and color-fixing group given by $H = \langle x, y, a^3, b\rangle \cong c2mm$ and $K = \langle x, y^2, a^3b\rangle \cong pm$, respectively. If we take $L = \langle x^3, x^4y^8\rangle \leq K$, then $N_G(L) = H$. This is an example of a non-perfectly colored tiling in $\mathbb{E}^2$ that yields a perfect coloring of the corresponding tiling $\mathbb{H}^*$ on $\mathbb{E}^2/L$. In this case, $H^* = N_H(L)/L \cong C_{24} \rtimes D_2$ and $K^* = N_K(L)/L \cong C_{12} \rtimes D_1$.

In the next section, we discuss the ideas on how $\mathbb{T}^*$ is realized in $\mathbb{E}^3$. This allows us to visualize $\mathbb{T}^*$ and its colorings using spatial figures and analyze their symmetry properties.

4. Geometric realizations of $\mathbb{T}^*$

4.1. Tiling $\overline{\mathbb{T}}$ on a round torus

Consider the tiling $\mathbb{T}^*$ on $\mathbb{E}^2/L$. Let $\mathbf{x}$, $\mathbf{y}$ be a pair of vectors corresponding to the translations x, $y \in T(G)$. Position $\mathbf{x}$, $\mathbf{y}$ in $\mathbb{T}$ and let $\mathbf{v}_1 = m_1\mathbf{x} + m_2\mathbf{y}$ and $\mathbf{v}_2 = n_1\mathbf{x} + n_2\mathbf{y}$.

The flat torus $\mathbb{E}^2/L$ can be embedded into the Cartesian product $S^1 \times S^1$ of two circles with circumferences $\|\mathbf{v}_2\|$ and $\|\mathbf{v}_1\|$ *via* the bijection

$$\varphi : \mathbb{E}^2/L \to S^1 \times S^1$$
$$Lu \mapsto \left[\frac{\|\mathbf{v}_2\|}{2\pi}\cos 2\pi p_2, \frac{\|\mathbf{v}_2\|}{2\pi}\sin 2\pi p_2, \frac{\|\mathbf{v}_1\|}{2\pi}\cos 2\pi p_1, \frac{\|\mathbf{v}_1\|}{2\pi}\sin 2\pi p_1\right],$$

where

$$p_1 = \frac{(\mathbf{u}\cdot\mathbf{v}_2)(\mathbf{v}_1\cdot\mathbf{v}_2) - (\mathbf{u}\cdot\mathbf{v}_1)(\mathbf{v}_2\cdot\mathbf{v}_2)}{(\mathbf{v}_1\cdot\mathbf{v}_2)^2 - (\mathbf{v}_1\cdot\mathbf{v}_1)(\mathbf{v}_2\cdot\mathbf{v}_2)}$$

and

$$p_2 = \frac{(\mathbf{u}\cdot\mathbf{v}_1)(\mathbf{v}_1\cdot\mathbf{v}_2) - (\mathbf{u}\cdot\mathbf{v}_2)(\mathbf{v}_1\cdot\mathbf{v}_1)}{(\mathbf{v}_1\cdot\mathbf{v}_2)^2 - (\mathbf{v}_1\cdot\mathbf{v}_1)(\mathbf{v}_2\cdot\mathbf{v}_2)}$$

refer to the coefficients of projection of the point u (viewed as a vector $\mathbf{u}$) in $\mathbb{E}^2$ onto $\mathbf{v}_1$ and $\mathbf{v}_2$, respectively, and $(\cdot)$ is the standard Euclidean inner product. It is straightforward to show that the map φ is well defined and is independent of $u \in Lu$. Since $S^1 \times S^1$ also lies in the 3-sphere S^3 of radius $(\|\mathbf{v}_1\|^2 + \|\mathbf{v}_2\|^2)^{1/2}/2\pi$ centered at the origin of the Euclidean 4-space $\mathbb{E}^4$, we can use a stereographic projection to project the image of $\mathbb{E}^2/L$ to $\mathbb{E}^3$. Specifically, we use

$$\psi : S^1 \times S^1 \to \mathbb{E}^3$$
$$\varphi(Lu) \mapsto \frac{\left[\|\mathbf{v}_2\|\cos 2\pi p_2, \|\mathbf{v}_2\|\sin 2\pi p_2, \|\mathbf{v}_1\|\sin 2\pi p_1\right]}{(\|\mathbf{v}_1\|^2 + \|\mathbf{v}_2\|^2)^{1/2} - \|\mathbf{v}_1\|\cos 2\pi p_1}.$$

The image of $\mathbb{E}^2/L$ under the composition $(\psi \circ \varphi)$ is a *round torus*. By applying $(\psi \circ \varphi)$ to the tiling $\mathbb{T}^*$, we obtain a tiling $\overline{\mathbb{T}}$ of the round torus whose vertices, edges and faces are the

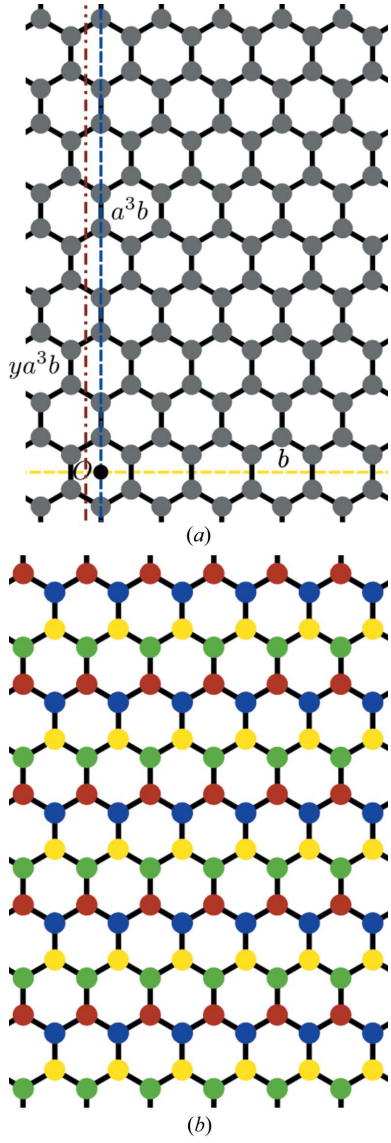

Figure 1
(*a*) An uncolored tiling $\mathbb{H}$ by regular hexagons with axes of the reflections b (yellow), a^3b (blue) and glide reflection ya^3b (red). (*b*) A non-perfect vertex 4-coloring of $\mathbb{H}$.

images under $(\psi \circ \varphi)$ of the vertices, edges and faces of $\mathbb{T}^*$. We refer to this tiling on the round torus as the *geometric realization* of $\mathbb{T}^*$ defined by $\mathbf{v}_1$ and $\mathbf{v}_2$. We can imagine $\overline{\mathbb{T}}$ as the result of rolling $\mathbb{T}$ along $\mathbf{v}_1$ to obtain a tiling on a cylinder with circumference $\|\mathbf{v}_1\|$, and then bending this cylinder along $\mathbf{v}_2$ to obtain a tiling on a round torus with *minor circle* of circumference $\|\mathbf{v}_1\|$ and *major circle* or *equator* of circumference $\|\mathbf{v}_2\|$.

We remark that if $\mathbf{v}_1$ and $\mathbf{v}_2$ are orthogonal, then φ is an isometric isomorphism and, hence, the composition $(\psi \circ \varphi)$ is conformal (Sullivan, 2011). In this case, $\overline{\mathbb{T}}$ is a conformal realization of $\mathbb{T}^*$ on the round torus. Otherwise, $\overline{\mathbb{T}}$ is a non-conformal realization and can be thought of as obtained by continuously deforming $\mathbb{T}$ first to force $\mathbf{v}_1$ and $\mathbf{v}_2$ to be orthogonal, before folding it into a round torus.

To illustrate the preceding notions, we have the following examples.

Consider the tiling $\mathbb{H}^*$ on $\mathbb{E}^2/L$ where $L = \langle x^3, x^4y^8 \rangle$. Choose the vectors $\mathbf{x}$, $\mathbf{y}$ so that they intersect at O as shown in Fig. 2(*a*). This gives us the orthogonal vectors $\mathbf{v}_1 = 3\mathbf{x}$ and $\mathbf{v}_2 = 4\mathbf{x} + 8\mathbf{y}$. If we apply the map $(\psi \circ \varphi)$ to $\mathbb{H}^*$, we obtain the conformal realization presented in Fig. 2(*b*).

As a second example, consider the tiling $\mathbb{H}^*$ on $\mathbb{E}^2/L$ where $L = \langle x^3, x^7y^8 \rangle$. We obtain the non-orthogonal vectors $\mathbf{v}_1' = \mathbf{v}_1$ and $\mathbf{v}_2' = 7\mathbf{x} + 8\mathbf{y}$ also shown in Fig. 2(*a*). The continuous deformation of $\mathbb{H}$ which forces $\mathbf{v}_1'$ and $\mathbf{v}_2'$ to be orthogonal is

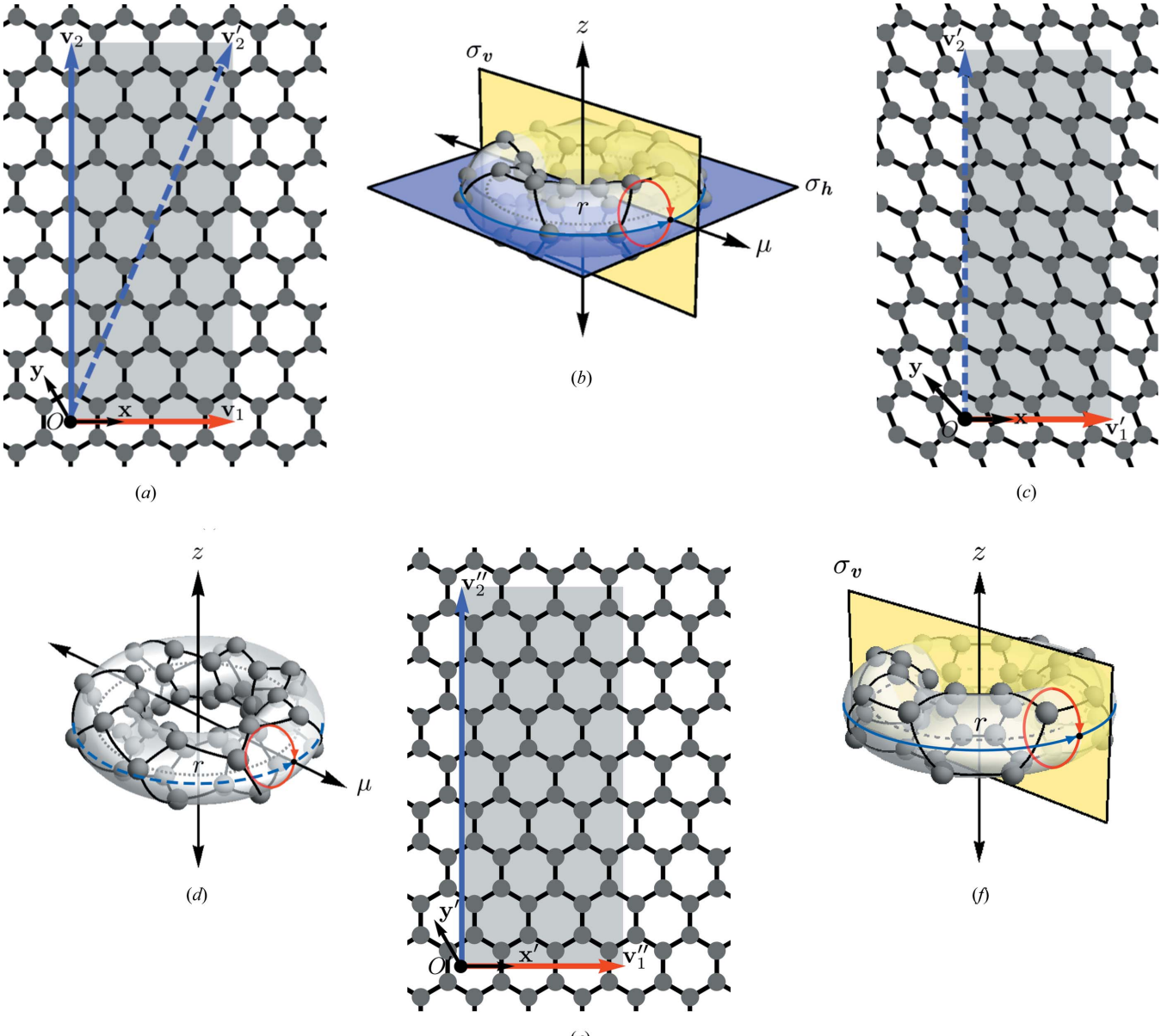

Figure 2
(*a*) A tiling $\mathbb{H}$ by regular hexagons with vectors $\mathbf{v}_1 = 3\mathbf{x}$, $\mathbf{v}_2 = 4\mathbf{x} + 8\mathbf{y}$ and $\mathbf{v}_2' = 7\mathbf{x} + 8\mathbf{y}$. (*b*) A conformal realization of $\mathbb{H}^*$ defined by $\mathbf{v}_1$ and $\mathbf{v}_2$. (*c*) A continuous deformation of the tiling in (*a*) that forces $\mathbf{v}_1' = \mathbf{v}_1$ and $\mathbf{v}_2'$ to be orthogonal. (*d*) A non-conformal realization of $\mathbb{H}^*$ defined by $\mathbf{v}_1'$ and $\mathbf{v}_2'$. (*e*) Vectors $\mathbf{v}_1'' = 3\mathbf{x}'$ and $\mathbf{v}_2'' = 4\mathbf{x}' + 8\mathbf{y}'$. (*f*) A conformal realization of $\mathbb{H}^*$ defined by $\mathbf{v}_1''$ and $\mathbf{v}_2''$.

Table 1
The seven axial point groups and their generators.

Axial point group	Minimal generating set	Abstract group
$\mathbf{C}_n$	ρ_n	C_n
$\mathbf{D}_n$	ρ_n, μ	D_n
$\mathbf{C}_{n\mathbf{h}}$	$\rho_n, \sigma_{\mathbf{h}}$	$C_n \times C_2$
$\mathbf{C}_{n\mathbf{v}}$	$\rho_n, \sigma_{\mathbf{v}}$	D_n
$\mathbf{S}_{2n}$	λ_{2n}	C_{2n}
$\mathbf{D}_{n\mathbf{d}}$	σ_v, λ_{2n}	D_{2n}
$\mathbf{D}_{n\mathbf{h}}$	$\rho_n, \sigma_{\mathbf{v}}, \sigma_{\mathbf{h}}$	$D_n \times C_2$, $C_n \rtimes D_2$

C_n – cyclic group of order n; D_n – dihedral group of order $2n$.

shown in Fig. 2(*c*). The resulting non-conformal realization of $\mathbb{H}^*$ is presented in Fig. 2(*d*).

Given the same L in the first example, we can obtain a different conformal realization by choosing $\mathbf{x}'$, $\mathbf{y}'$ so that they intersect at O' as shown in Fig. 2(*e*). By doing so, we obtain the orthogonal vectors $\mathbf{v}_1'' = 3\mathbf{x}'$ and $\mathbf{v}_2'' = 4\mathbf{x}' + 8\mathbf{y}'$. These vectors define the conformal realization of $\mathbb{H}^*$ presented in Fig. 2(*f*).

In each of Figs. 2(*b*), 2(*d*) and 2(*f*), the minor and major circles of the round torus are colored red and blue, respectively.

4.2. Symmetry group of $\overline{\mathbb{T}}$

Since the stereographic projection ψ is conformal but not isometric, the composition $(\psi \circ \varphi)$ is not an isometry. In fact, a flat torus cannot be isometrically embedded into a round torus (O'Neill, 2006; Sullivan, 2011). Thus, the symmetry group of $\overline{\mathbb{T}}$, which we denote by $\overline{G}$ (isometries of $\mathbb{E}^3$ that leave $\overline{\mathbb{T}}$ invariant), is not isomorphic to the symmetry group $G^* \cong N_G(L)/L$ of $\mathbb{T}^*$. Nevertheless, each symmetry in G^* corresponds to a motion of $\overline{\mathbb{T}}$ that maps face boundaries to face boundaries (Senechal, 1988). Thus, G^* contains an isomorphic copy of $\overline{G}$.

By nature, each of the isometries in $\overline{G}$ must fix the *principal rotation axis z* and the *ring axis r* of the round torus (Fig. 2*b*). In addition, since $\overline{\mathbb{T}}$ is a tiling on a finite surface, $\overline{G}$ is necessarily finite. As such, $\overline{G}$ is isomorphic to one of the seven *axial point groups* (Table 1). Axial point groups are exactly the common finite subgroups of the full symmetry group $\mathbf{D}_{\infty\mathbf{h}}$ of the round torus and the orthogonal group $O(3)$ of dimension 3. Consequently, $\overline{G}$ may contain only the following types of isometries: rotation about the z axis; reflection in the *equatorial plane* (the plane containing the r axis); reflection in a plane passing through the z axis; twofold rotation about an axis lying in the equatorial plane; and rotoinversion about the center of the round torus (the point of intersection of the z axis and the equatorial plane).

The elements of $\overline{G}$ may be determined by identifying planar symmetries in $N_G(L)$ that become axial symmetries when $\mathbb{T}$ is folded to form $\overline{\mathbb{T}}$. Note that the translation $x^{\frac{n_1}{n}}y^{\frac{n_2}{n}}$, where $n = \gcd(n_1, n_2)$, yields an n-fold rotation ρ_n about the z axis. Thus, $\overline{G}$ always contains ρ_n and hence contains a subgroup isomorphic to $\mathbf{C}_n$. Now to check for other axial symmetries in $\overline{G}$ we take into account $\mathbf{v}_2$. Since $\mathbf{v}_2$ becomes the major circle of the round torus, we use as a basis the position of the vector, center or axis of a translation, rotation or reflection/glide reflection, respectively, relative to $\mathbf{v}_2$ in determining whether the particular symmetry becomes an axial symmetry.

If there is a translation in $N_G(L)$ whose vector is parallel to or coincides with $\mathbf{v}_2$, then this translation becomes a rotation about the z axis (a power of ρ_n). If a twofold rotation in $N_G(L)$ has a center lying on $\mathbf{v}_2$, then we get a twofold rotation about an axis lying in the equatorial plane. We denote one such rotation by μ.

Other axial symmetries arise when $\mathbf{v}_1$ is orthogonal to $\mathbf{v}_2$. Suppose there is a reflection in $N_G(L)$. If the axis of reflection contains $\mathbf{v}_2$, then this reflection becomes the reflection $\sigma_{\mathbf{h}}$ in the equatorial plane. If the axis is perpendicular to $\mathbf{v}_2$, on the other hand, we obtain a reflection in a plane containing the z axis. We denote one such reflection by $\sigma_{\mathbf{v}}$. Lastly, a glide reflection in $N_G(L)$ with axis containing $\mathbf{v}_2$ becomes a rotoinversion about the center of the torus. In particular, a glide reflection whose translation component is $x^{\frac{n_1}{2n}}y^{\frac{n_2}{2n}}$ yields an n-fold rotoinversion λ_{2n} about the center of the torus.

No other axial symmetries arise when $\mathbf{v}_1$ is not orthogonal to $\mathbf{v}_2$. This is an inevitable consequence of the deformation of $\mathbb{T}$ resulting from the map $(\psi \circ \varphi)$, which destroys axes of symmetries.

The above discussion is summarized in Table 2.

Theorems 3–4 characterize $\overline{G}$ based on the symmetries present in $N_G(L)$. In Fig. 3, we present unit cells of $N_G(L)$ (Schattschneider, 1978) together with $\mathbf{v}_1$, $\mathbf{v}_2$. Before proving the theorems, we first state and prove the following lemma.

Lemma 1. Suppose $\mathbf{v}_1$, $\mathbf{v}_2$ are orthogonal. If $N_G(L)$ contains a rotation with angle θ radians, then $\theta = k\pi/2$, where $k = 0, 1, 2$ or 3. The case when $k = 1$ or 3 happens only if $\|\mathbf{v}_1\| = \|\mathbf{v}_2\|$.

Proof. Let $(\mathbf{t}, \alpha)$ be a rotation in $N_G(L)$ with vector component $\mathbf{t}$ and orthogonal component α. Then the vector component $\alpha\mathbf{v}_2$ of $(\mathbf{t}, \alpha)(\mathbf{v}_2, id)(\mathbf{t}, \alpha)^{-1} = (\alpha\mathbf{v}_2, id) \in L$ is in the lattice Λ spanned by $\mathbf{v}_1$ and $\mathbf{v}_2$. Since $\mathbf{v}_1$ and $\mathbf{v}_2$ are orthogonal, Λ must either be square or rectangular. Thus, $\mathbf{v}_1$ and $\mathbf{v}_2$ are vectors of minimal lengths in Λ. It follows that either $\alpha\mathbf{v}_2 = \mathbf{v}_2$, $\alpha\mathbf{v}_2 = -\mathbf{v}_2$, $\alpha\mathbf{v}_2 = \mathbf{v}_1$ or $\alpha\mathbf{v}_2 = -\mathbf{v}_1$. Let θ be the angle of rotation of $(\mathbf{t}, \alpha)$. If $\alpha\mathbf{v}_2 = \mathbf{v}_2$ or $\alpha\mathbf{v}_2 = -\mathbf{v}_2$, then $\theta = 0$ or π. If $\alpha\mathbf{v}_2 = \mathbf{v}_1$ or $\alpha\mathbf{v}_2 = -\mathbf{v}_1$, on the other hand, then $\theta = \pi/2$ or $3\pi/2$. Because α preserves distance, $\alpha\mathbf{v}_2 = \mathbf{v}_1$ or $\alpha\mathbf{v}_2 = -\mathbf{v}_1$ happens only if $\|\mathbf{v}_1\| = \|\mathbf{v}_2\|$. □

As a consequence of Lemma 1, we see that if L corresponds to a pair of orthogonal vectors, then $N_G(L)$ cannot be isomorphic to a crystallographic group of type $p3$, $p3m1$, $p31m$, $p6$ or $p6mm$. In Theorem 3 below, we do not consider these crystallographic group types in our analyses.

Theorem 3. Suppose $\mathbf{v}_1$, $\mathbf{v}_2$ are orthogonal.

(i) If $N_G(L)$ contains reflections in a single direction, then $\overline{G} \cong \mathbf{C}_n$, $\mathbf{S}_{2n}$, $\mathbf{D}_n$, $\mathbf{C}_{n\mathbf{v}}$, $\mathbf{C}_{n\mathbf{h}}$ or $\mathbf{D}_{n\mathbf{d}}$.

(ii) If $N_G(L)$ contains reflections in more than one direction, then $\overline{G} \cong \mathbf{C}_n$, $\mathbf{S}_{2n}$, $\mathbf{D}_n$, $\mathbf{C}_{n\mathbf{v}}$, $\mathbf{D}_{n\mathbf{d}}$ or $\mathbf{D}_{n\mathbf{h}}$.

(iii) If $N_G(L)$ does not contain any reflection, then $\overline{G} \cong \mathbf{C}_n$, $\mathbf{S}_{2n}$ or $\mathbf{D}_n$.

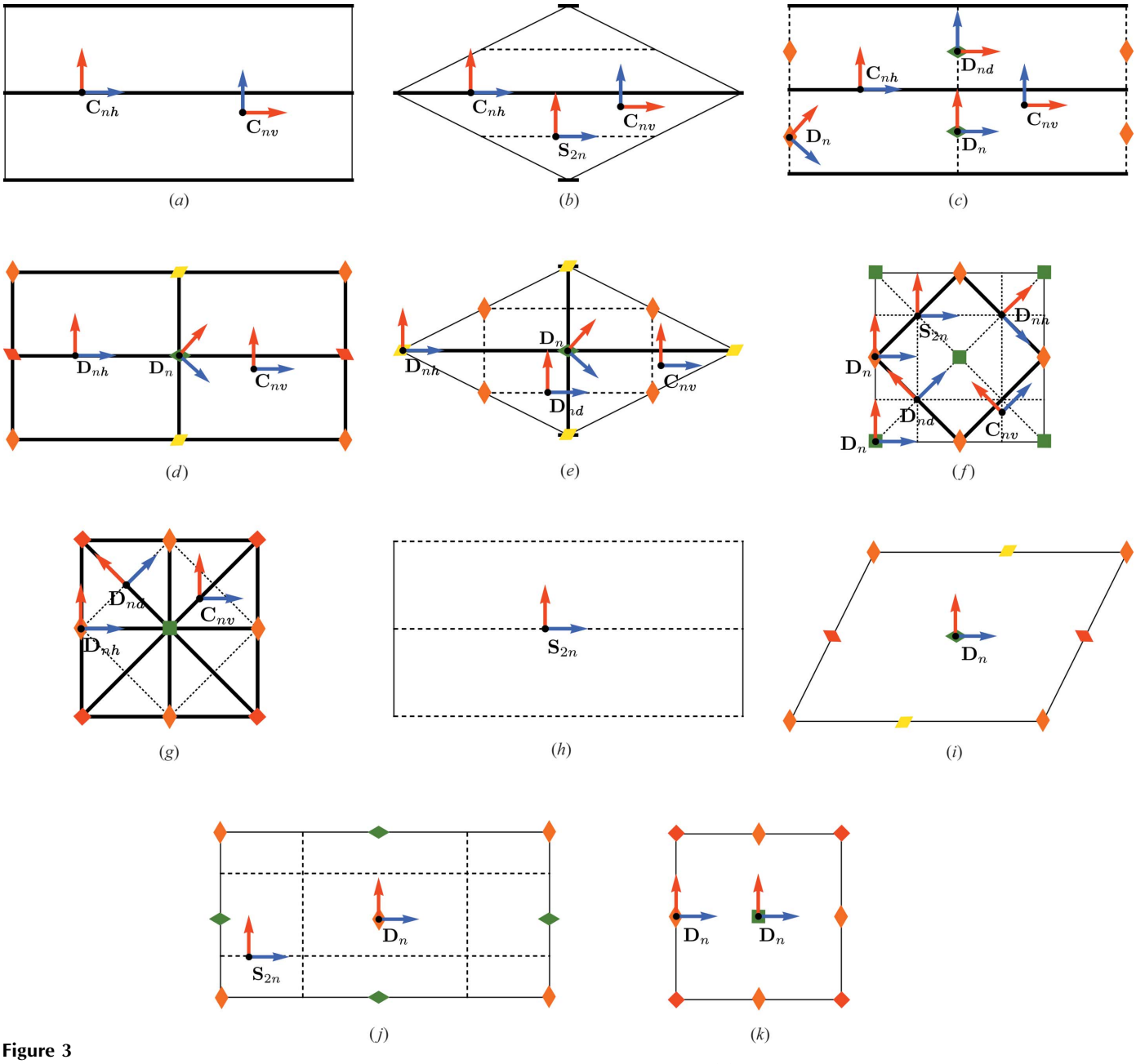

Figure 3
Different positions of the orthogonal vectors $\mathbf{v}_1$ (red) and $\mathbf{v}_2$ (blue) drawn in a unit cell of $N_G(L)$. The bold lines represent reflection axes; the dashed lines represent glide axes; the diamonds and squares represent centers of twofold and fourfold rotations, respectively. (*a*) $N_G(L) \cong pm$, (*b*) $N_G(L) \cong cm$, (*c*) $N_G(L) \cong p2mg$, (*d*) $N_G(L) \cong p2mm$, (*e*) $N_G(L) \cong c2mm$, (*f*) $N_G(L) \cong p4mg$, (*g*) $N_G(L) \cong p4mm$, (*h*) $N_G(L) \cong pg$, (*i*) $N_G(L) \cong p2$, (*j*) $N_G(L) \cong p2gg$, (*k*) $N_G(L) \cong p4$.

Proof. (i) Suppose $N_G(L)$ contains reflections in a single direction. Then $N_G(L) \cong pm, p2mg$ or cm. If there is an axis of glide reflection that contains $\mathbf{v}_2$, then we obtain a rotoinversion λ_{2n} that is a generator of $\overline{G}$. Additionally, if there is an axis of reflection that is perpendicular to $\mathbf{v}_2$, we obtain a reflection $\sigma_{\mathbf{v}}$, a second generator of $\overline{G}$. In either case, $\overline{G} = \langle \lambda_{2n} \rangle \cong \mathbf{S}_{2n}$ or $\overline{G} = \langle \sigma_{\mathbf{v}}, \lambda_{2n} \rangle \cong \mathbf{D}_{n\mathbf{d}}$ (Figs. 3*b*–3*c*).

If no axis of glide reflection contains $\mathbf{v}_2$, then we have four cases. If a reflection axis is perpendicular to $\mathbf{v}_2$, then we obtain $\sigma_{\mathbf{v}}$. Together with ρ_n, we have $\overline{G} = \langle \rho_n, \sigma_{\mathbf{v}} \rangle \cong \mathbf{C}_{n\mathbf{v}}$. If a reflection axis contains $\mathbf{v}_2$, we obtain the reflection $\sigma_{\mathbf{h}}$ and hence $\overline{G} = \langle \rho_n, \sigma_{\mathbf{h}} \rangle \cong \mathbf{C}_{n\mathbf{h}}$. If the center of a twofold rotation lies on $\mathbf{v}_2$, we obtain a twofold rotation μ. Thus, $\overline{G} = \langle \rho_n, \mu \rangle \cong \mathbf{D}_n$. Otherwise, $\overline{G} = \langle \rho_n \rangle \cong \mathbf{C}_n$ (Figs. 3*a*–3*c*).

(ii) Suppose $N_G(L)$ contains reflections in more than one direction. Then $N_G(L) \cong p2mm$, $c2mm$, $p4mg$ or $p4mm$. If there is an axis of glide reflection containing $\mathbf{v}_2$, then using the arguments in the proof of (i), either $\overline{G} \cong \mathbf{S}_{2n}$ or $\overline{G} \cong \mathbf{D}_{n\mathbf{d}}$ (Figs. 3*e*–3*f*).

If no axis of glide reflection contains $\mathbf{v}_2$, the situations that occur are as follows. If a reflection axis is perpendicular to $\mathbf{v}_2$, we obtain $\sigma_{\mathbf{v}}$. If another reflection axis also contains $\mathbf{v}_2$, then $\sigma_{\mathbf{h}}$ is also contained in $\overline{G}$. In these cases, either $\overline{G} = \langle \rho_n, \sigma_{\mathbf{v}} \rangle \cong \mathbf{C}_{n\mathbf{v}}$ or $\overline{G} = \langle \rho_n, \sigma_{\mathbf{v}}, \sigma_{\mathbf{h}} \rangle \cong \mathbf{D}_{n\mathbf{h}}$. Suppose now that

Table 2
Correspondence between planar symmetries in $N_G(L)$ and axial symmetries in $\overline{G}$.

Planar symmetry	Special position	Axial symmetry
Translation	With vector parallel to or coinciding with $\mathbf{v}_2$	Rotation about the z axis
Twofold rotation	With center lying on $\mathbf{v}_2$	Twofold rotation about an axis lying in the equatorial plane
Reflection	With axis perpendicular to $\mathbf{v}_2$	Reflection in a plane containing the z axis
	With axis containing $\mathbf{v}_2$	Reflection in the equatorial plane
Glide reflection	With axis containing $\mathbf{v}_2$	Rotoinversion about center of the torus

no reflection axis is perpendicular to $\mathbf{v}_2$. If the center of a twofold rotation lies on $\mathbf{v}_2$, we have $\overline{G} \cong \mathbf{D}_n$. Otherwise, $\overline{G} \cong \mathbf{C}_n$ (Figs. 3*d*–3*g*).

(iii) Suppose $N_G(L)$ does not contain any reflection. Then $N_G(L) \cong p1$, pg, $p2$, $p2gg$ or $p4$. A check for an axis of glide reflection containing $\mathbf{v}_2$, or a center of twofold rotation lying on $\mathbf{v}_2$ is carried out. The proof follows the same arguments in the proof of (i) (Figs. 3*h*–3*k*). □

The axial-point-group type of $\overline{G}$ when $\mathbf{v}_1$, $\mathbf{v}_2$ are non-orthogonal is stated in the next theorem. The proof of this theorem is immediate.

Theorem 4. Suppose $\mathbf{v}_1, \mathbf{v}_2$ are non-orthogonal. If a center of a twofold rotation lies on $\mathbf{v}_2$, then $\overline{G} \cong \mathbf{D}_n$, otherwise $\overline{G} \cong \mathbf{C}_n$.

The results of Theorems 3–4 are summarized in Table 3.

The theorems are applied to determine $\overline{G}$ for the three examples discussed previously in §4.1. Note that, for all three, $N_G(L) = \langle x, y, a^3, b\rangle \cong c2mm$.

For the first one, since $\mathbf{v}_1$, $\mathbf{v}_2$ are orthogonal and $N_G(L)$ contains reflections in more than one direction, we use Theorem 3(ii). Since $\mathbf{v}_2$ is perpendicular to the reflection axis of b and is contained in the reflection axis of a^3b (Fig. 1*a*), the symmetry group of the tiling in Fig. 2(*b*) is $\overline{G} = \langle \rho_4, \sigma_{\mathbf{v}}, \sigma_{\mathbf{h}}\rangle \cong \mathbf{D}_{4\mathbf{h}}$.

The second example pertains to the case when $\mathbf{v}_1'$, $\mathbf{v}_2'$ are non-orthogonal. Note that the center O of the twofold rotation a^3 lies on $\mathbf{v}_2'$. By Theorem 4, the symmetry group of the tiling in Fig. 2(*d*) is $\overline{G}' = \langle \rho_1, \mu\rangle \cong \mathbf{D}_1$.

The third example pertains to the case when $\mathbf{v}_1''$, $\mathbf{v}_2''$ are the same as the vectors $\mathbf{v}_1$, $\mathbf{v}_2$ but moved to a different position. In this case, Theorem 3(ii) is again applicable. Since $\mathbf{v}_2''$ is contained in the axis of the glide reflection ya^3b and is perpendicular to the reflection axis of b as shown in Fig. 1(*a*), the theorem implies that the symmetry group of the tiling in Fig. 2(*f*) is $\overline{G}'' = \langle \sigma_{\mathbf{v}}, \lambda_8\rangle \cong \mathbf{D}_{4\mathbf{d}}$.

From a group-theoretic perspective, it is interesting to see how the abstract group structure of $\overline{G}$ (refer to Table 1) relates to that of G^*. For instance, consider each of the three symmetry groups $\overline{G}$, $\overline{G}'$ and $\overline{G}''$ discussed in the preceding examples above arising from $G^* \cong C_{24} \rtimes D_2$. To see the relation, we decompose each symmetry group as a semidirect product of subgroups of C_{24} and D_2. In the first example, we have $\overline{G} \cong \mathbf{D}_{4\mathbf{h}} \cong C_4 \rtimes D_2$, where $C_4 \cong \langle \rho_4\rangle$ and $D_2 \cong \langle \sigma_{\mathbf{v}}, \sigma_{\mathbf{h}}\rangle$. In the second one, we have $\overline{G}' \cong \mathbf{D}_1 \cong D_1$, which can also be written as $C_1 \rtimes D_1$, where $C_1 \cong \langle \rho_1\rangle$ and $D_1 \cong \langle \mu\rangle$. Finally, in the third example, we have $\overline{G}'' \cong \mathbf{D}_{4\mathbf{d}} \cong D_8$, which is decomposable as $C_8 \rtimes D_1$, where $C_8 \cong \langle \lambda_8\rangle$ and $D_1 \cong \langle \sigma_{\mathbf{v}}\rangle$. Similar decompositions may be easily accomplished for symmetry groups of types $\mathbf{C}_n$ and $\mathbf{C}_{n\mathbf{v}}$, which can also arise when $N_G(L) \cong c2mm$ (refer to Table 3).

5. Geometric model of nanotori

In theory, a carbon nanotorus is a nanosized material obtained when a hexagonal monolayer of carbon atoms (*graphene*) is rolled into a cylindrical tube along $\mathbf{v}_1$ (the transverse vector) and then joined end to end along $\mathbf{v}_2$ (the longitudinal vector) to form a toroidal nanostructure (Arezoomand & Taeri, 2009).

In this work, a geometric model of a carbon nanotorus is obtained as follows. Consider a tiling by regular hexagons $\mathbb{H} = (6^3)$ with symmetry group $G = \langle x, y, a, b\rangle \cong p6mm$ and a pair of generating translations for L corresponding to a pair of orthogonal vectors $\mathbf{v}_1 = m_1\mathbf{x} + m_2\mathbf{y}$ and $\mathbf{v}_2 = n_1\mathbf{x} + n_2\mathbf{y}$, where $(2m_1 - m_2)n_1 + (2m_2 - m_1)n_2 = 0$. Then the tiling $\overline{\mathbb{H}}$ on the round torus defined by $\mathbf{v}_1$ and $\mathbf{v}_2$ models a $(m_1 - m_2, m_2, n_1 - n_2, n_2)$ *carbon nanotorus*. The vertices of the tiling represent carbon atoms and the edges represent atomic bonds.

Table 4 lists the subgroups L which give rise to models of carbon nanotori. For each L, we provide the group G^* and the various possible symmetry groups $\overline{G}$ of the corresponding carbon nanotorus. We remark that the orthogonality restriction imposed on $\mathbf{v}_1$ and $\mathbf{v}_2$ implies that $\|\mathbf{v}_1\| \neq \|\mathbf{v}_2\|$.

Fig. 2(*b*) shows a model of a $(3, 0, -4, 8)$ carbon nanotorus with $G^* \cong C_{24} \rtimes D_2$ and $\overline{G} \cong \mathbf{D}_{4\mathbf{h}}$.

Table 3
Possible axial-point-group types for the symmetry group $\overline{G}$ of $\overline{\mathbb{T}}$ defined by $\mathbf{v}_1$ and $\mathbf{v}_2$.

The symbol (−) indicates non-applicability.

	$\overline{G}$	
$N_G(L)$	Orthogonal	Non-orthogonal
$p1$	$\mathbf{C}_n$	$\mathbf{C}_n$
$p2$	$\mathbf{C}_n$, $\mathbf{D}_n$	$\mathbf{C}_n$, $\mathbf{D}_n$
$p3$	−	$\mathbf{C}_n$
$p4$	$\mathbf{C}_n$, $\mathbf{D}_n$	$\mathbf{C}_n$, $\mathbf{D}_n$
$p6$	−	$\mathbf{C}_n$, $\mathbf{D}_n$
pg	$\mathbf{C}_n$, $\mathbf{S}_{2n}$	$\mathbf{C}_n$
$p2gg$	$\mathbf{C}_n$, $\mathbf{S}_{2n}$, $\mathbf{D}_n$	$\mathbf{C}_n$, $\mathbf{D}_n$
pm	$\mathbf{C}_n$, $\mathbf{C}_{n\mathbf{v}}$, $\mathbf{C}_{n\mathbf{h}}$	$\mathbf{C}_n$
cm	$\mathbf{C}_n$, $\mathbf{S}_{2n}$, $\mathbf{C}_{n\mathbf{v}}$, $\mathbf{C}_{n\mathbf{h}}$	$\mathbf{C}_n$
$p2mg$	$\mathbf{C}_n$, $\mathbf{D}_n$, $\mathbf{C}_{n\mathbf{v}}$, $\mathbf{C}_{n\mathbf{h}}$, $\mathbf{D}_{n\mathbf{d}}$	$\mathbf{C}_n$, $\mathbf{D}_n$
$p2mm$	$\mathbf{C}_n$, $\mathbf{D}_n$, $\mathbf{C}_{n\mathbf{v}}$, $\mathbf{D}_{n\mathbf{h}}$	$\mathbf{C}_n$, $\mathbf{D}_n$
$c2mm$	$\mathbf{C}_n$, $\mathbf{D}_n$, $\mathbf{C}_{n\mathbf{v}}$, $\mathbf{D}_{n\mathbf{d}}$, $\mathbf{D}_{n\mathbf{h}}$	$\mathbf{C}_n$, $\mathbf{D}_n$
$p3m1$	−	$\mathbf{C}_n$
$p31m$	−	$\mathbf{C}_n$
$p4mg$	$\mathbf{C}_n$, $\mathbf{S}_{2n}$, $\mathbf{D}_n$, $\mathbf{C}_{n\mathbf{v}}$, $\mathbf{D}_{n\mathbf{d}}$, $\mathbf{D}_{n\mathbf{h}}$	$\mathbf{C}_n$, $\mathbf{D}_n$
$p4mm$	$\mathbf{C}_{n\mathbf{v}}$, $\mathbf{D}_{n\mathbf{d}}$, $\mathbf{D}_{n\mathbf{h}}$	$\mathbf{C}_n$, $\mathbf{D}_n$
$p6mm$	−	$\mathbf{C}_n$, $\mathbf{D}_n$

Table 4
Symmetry groups of carbon nanotori.

$L = \langle x^{m_1}y^{m_2}, x^{n_1}y^{n_2}\rangle$	$N_G(L)$	G^*	$\overline{G}$
$m_2 = 0$ and $2n_1 = n_2$	$\langle x, y, b, a^3b\rangle \cong c2mm$	$(C_d \times C_{2mn/d}) \rtimes D_2$	$\mathbf{C}_{nv}$, $\mathbf{D}_{nd}$, $\mathbf{D}_{nh}$
$2m_1 = m_2$ and $n_2 = 0$	$\langle x, y, b, a^3b\rangle \cong c2mm$	$(C_d \times C_{2mn/d}) \rtimes D_2$	$\mathbf{C}_{nv}$, $\mathbf{D}_{nd}$, $\mathbf{D}_{nh}$
$m_1 = m_2$ and $n_1 = -n_2$	$\langle x, y, a^2b, a^5b\rangle \cong c2mm$	$(C_d \times C_{2mn/d}) \rtimes D_2$	$\mathbf{C}_{nv}$, $\mathbf{D}_{nd}$, $\mathbf{D}_{nh}$
$m_1 = -m_2$ and $n_1 = n_2$	$\langle x, y, a^2b, a^5b\rangle \cong c2mm$	$(C_d \times C_{2mn/d}) \rtimes D_2$	$\mathbf{C}_{nv}$, $\mathbf{D}_{nd}$, $\mathbf{D}_{nh}$
$m_1 = 0$ and $n_1 = 2n_2$	$\langle x, y, ab, a^4b\rangle \cong c2mm$	$(C_d \times C_{2mn/d}) \rtimes D_2$	$\mathbf{C}_{nv}$, $\mathbf{D}_{nd}$, $\mathbf{D}_{nh}$
$m_1 = 2m_2$ and $n_1 = 0$	$\langle x, y, ab, a^4b\rangle \cong c2mm$	$(C_d \times C_{2mn/d}) \rtimes D_2$	$\mathbf{C}_{nv}$, $\mathbf{D}_{nd}$, $\mathbf{D}_{nh}$
Other values	$\langle x, y, a^3\rangle \cong p2$	$(C_d \times C_{\lvert m_1n_2 - m_2n_1\rvert/d}) \rtimes C_2$	$\mathbf{C}_n$, $\mathbf{D}_n$

$(2m_1 - m_2)n_1 + (2m_2 - m_1)n_2 = 0$, $d = \gcd(m_1, m_2, n_1, n_2)$, $m = \gcd(m_1, m_2)$, $n = \gcd(n_1, n_2)$.

There are two special motions of a carbon nanotorus that preserve the ring axis but not the principal rotation axis – the *whirling motion* and the *torus screw rotation*. These motions are not distance preserving and hence are not elements of $\overline{G}$. Nevertheless, we can regard them as four-dimensional symmetries in G^* acting on $\mathbb{H}^*$ with analogous effects as three-dimensional non-rigid motions acting on the nanotorus. In related literature (Bovin *et al.*, 2001; Arezoomand & Taeri, 2009; Zhao *et al.*, 2012), these are also considered as symmetry elements.

An m-fold whirling motion ω_m about the r axis can be described as a 'rotation' of a nanotorus about r. It is brought about by a translation in $N_G(L)$ with vector perpendicular to $\mathbf{v}_2$. It sends points near the equator to points near the center of the torus, and conversely, *via* circular paths (Fig. 4*a*). One such whirling motion corresponds to the element $L(x^{\frac{m_1}{m}}y^{\frac{m_2}{m}})$ of order $m = \gcd(m_1, m_2)$ in G^*.

A *torus screw rotation* ζ_p^q about the r axis, on the other hand, is a composition of a whirling motion by an angle of $2\pi/p$ about r and a rotation by an angle of $2\pi/q$ about the principal rotation axis z. It results from a translation in $N_G(L)$ with vector neither coinciding with nor parallel or perpendicular to $\mathbf{v}_2$. It sends points near the equator to points near the center of the torus, and conversely, *via* a helical path (Fig. 4*b*). One such torus screw rotation corresponds to an element of order $|m_1n_2 - m_2n_1|/d$ in G^*.

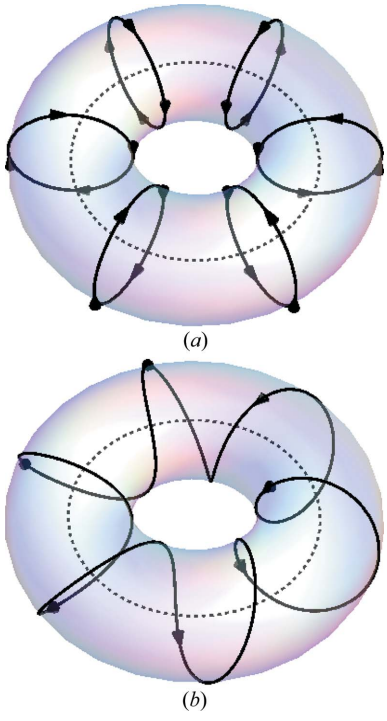

Figure 4
(*a*) Oriented circular paths depicting a whirling motion. (*b*) An oriented helical path depicting a torus screw rotation.

If we consider the tiling $\mathbb{H}$ with its vertices assigned more than one color and fold it into a round torus, then we obtain a model of a *structural analog* of a carbon nanotorus. By a structural analog, we mean a toroidal nanomaterial with the same geometric structure as that of a carbon nanotorus but made up of different atoms. The symmetry group $\overline{K}$ of a structural analog consists of axial symmetries of the colored tiling $\overline{\mathbb{H}}$ on the round torus. It is obtained by looking at the symmetries in $N_K(L)$ that become axial symmetries following the same arguments in the previous section. The whirling motions and torus screw rotations of a structural analog can be regarded as elements of K^*.

Let us take, for example, the vertex 4-coloring of $\mathbb{H}$ with color-fixing group $K = \langle x, y^2, a^3b\rangle \cong pm$ appearing in Fig. 1(*b*). Using $L = \langle x^3, x^4y^8\rangle \leq K$ with $N_K(L) = K$, we obtain a geometric model of a structural analog of the $(3, 0, -4, 8)$ carbon nanotorus in Fig. 2(*b*). This analog shown in Fig. 5 is composed of four different types of atoms (48 in all) that occur in the same number. The symmetry group of this structural analog is $\overline{K} = \langle \rho_4, \sigma_{\mathbf{h}}\rangle \cong \mathbf{C}_{4\mathbf{h}}$. The non-rigid motions of this nanotorus include the threefold whirling motion ω_3 and the torus screw rotation ζ_3^4 corresponding, respectively, to the elements Lx of order 3 and Lx^2y^2 of order 12 in $K^* \cong C_{12} \rtimes D_1$.

In Fig. 6, we present boron carbon nitride ($B_xC_yN_z$) hexagonal monolayers represented by vertex colorings of $\mathbb{H}$. We remark that boron nitride nanotori, which can be obtained from the BN monolayer in Fig. 6(*a*), have been investigated very recently in Loh & Baillargeat (2013). Using Theorem 3, we are able to determine for each L the group K^* and the possible symmetry group $\overline{K}$ of the boron carbon nitride nanotori that will arise from these monolayers. The groups are listed in Table 5.

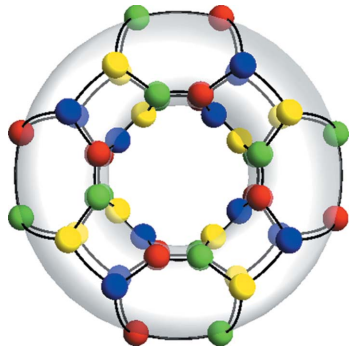

Figure 5
A structural analog of the $(3, 0, -4, 8)$ carbon nanotorus in Fig. 2(*b*).

Table 5
Symmetry groups of boron carbon nitride nanotori.

	BN (Fig. 6*a*)			BC_3 (Fig. 6*b*)			BCN (Fig. 6*c*)			BC_2N (type I) (Fig. 6*d*)			BC_2N (type II) (Fig. 6*e*)		
$L = \langle x^{m_1}y^{m_2}, x^{n_1}y^{n_2}\rangle$	$N_K(L)$	K^*	$\overline{K}$	$N_K(L)$	K^*	$\overline{K}$	$N_K(L)$	K^*	$\overline{K}$	$N_K(L)$	K^*	$\overline{K}$	$N_K(L)$	K^*	$\overline{K}$
$m_2 = 0$ and $2n_1 = n_2$	*cm*	K_1^*	$\mathbf{C}_n$, $\mathbf{S}_{2n}$, $\mathbf{C}_{nh}$	*c2mm*	K_3^*	$\mathbf{C}_{nv}$, $\mathbf{D}_{nd}$, $\mathbf{D}_{nh}$	*pm*	K_1^*	$\mathbf{C}_n$, $\mathbf{C}_{nh}$	*p2mm*	K_3^*	$\mathbf{C}_{nv}$, $\mathbf{D}_{nh}$	*pm*	K_1^*	$\mathbf{C}_n$, $\mathbf{C}_{nh}$
$2m_1 = m_2$ and $n_2 = 0$	*cm*	K_1^*	$\mathbf{C}_n$, $\mathbf{C}_{nv}$	*c2mm*	K_3^*	$\mathbf{C}_{nv}$, $\mathbf{D}_{nd}$, $\mathbf{D}_{nh}$	*pm*	K_1^*	$\mathbf{C}_n$, $\mathbf{C}_{nh}$	*p2mm*	K_3^*	$\mathbf{C}_{nv}$, $\mathbf{D}_{nh}$	*pm*	K_1^*	$\mathbf{C}_n$, $\mathbf{C}_{nh}$
$m_1 = m_2$ and $n_1 = -n_2$	*cm*	K_1^*	$\mathbf{C}_n$, $\mathbf{S}_{2n}$, $\mathbf{C}_{nh}$	*c2mm*	K_3^*	$\mathbf{C}_{nv}$, $\mathbf{D}_{nd}$, $\mathbf{D}_{nh}$	*p1*	K_2^*	$\mathbf{C}_n$	*p2*	K_4^*	$\mathbf{C}_n$, $\mathbf{D}_n$	*p1*	K_2^*	$\mathbf{C}_n$
$m_1 = -m_2$ and $n_1 = n_2$	*cm*	K_1^*	$\mathbf{C}_n$, $\mathbf{C}_{nv}$	*c2mm*	K_3^*	$\mathbf{C}_{nv}$, $\mathbf{D}_{nd}$, $\mathbf{D}_{nh}$	*p1*	K_2^*	$\mathbf{C}_n$	*p2*	K_4^*	$\mathbf{C}_n$, $\mathbf{D}_n$	*p1*	K_2^*	$\mathbf{C}_n$
$m_1 = 0$ and $n_1 = 2n_2$	*cm*	K_1^*	$\mathbf{C}_n$, $\mathbf{S}_{2n}$, $\mathbf{C}_{nh}$	*c2mm*	K_3^*	$\mathbf{C}_{nv}$, $\mathbf{D}_{nd}$, $\mathbf{D}_{nh}$	*p1*	K_2^*	$\mathbf{C}_n$	*p2*	K_4^*	$\mathbf{C}_n$, $\mathbf{D}_n$	*p1*	K_2^*	$\mathbf{C}_n$
$m_1 = 2m_2$ and $n_1 = 0$	*cm*	K_1^*	$\mathbf{C}_n$, $\mathbf{C}_{nv}$	*c2mm*	K_3^*	$\mathbf{C}_{nv}$, $\mathbf{D}_{nd}$, $\mathbf{D}_{nh}$	*p1*	K_2^*	$\mathbf{C}_n$	*p2*	K_4^*	$\mathbf{C}_n$, $\mathbf{D}_n$	*p1*	K_2^*	$\mathbf{C}_n$
Other values	*p1*	K_2^*	$\mathbf{C}_n$	*p2*	K_4^*	$\mathbf{C}_n$, $\mathbf{D}_n$	*p1*	K_2^*	$\mathbf{C}_n$	*p2*	K_4^*	$\mathbf{C}_n$, $\mathbf{D}_n$	*p1*	K_2^*	$\mathbf{C}_n$

$(2m_1 - m_2)n_1 + (2m_2 - m_1)n_2 = 0$, $d = \gcd(m_1, m_2, n_1, n_2)$, $m = \gcd(m_1, m_2)$, $n = \gcd(n_1, n_2)$. $K_1^* \cong (C_d \times C_{2mn/d}) \rtimes D_1$; $K_2^* \cong C_d \times C_{|m_1n_2 - m_2n_1|/d}$; $K_3^* \cong (C_d \times C_{2mn/d}) \rtimes D_2$; $K_4^* \cong (C_d \times C_{|m_1n_2 - m_2n_1|/d}) \rtimes C_2$.

Generating the vertex colorings of $\mathbb{H}$ employed to model structural analogs in this paper was facilitated by a coloring framework found in De Las Peñas *et al.* (2006, 2011). The framework was translated into *GAP* (The GAP Group, 2013) and *Mathematica* (Wolfram Research, 2011) codes to arrive at these colorings and render them as three-dimensional graphics.

Other theoretical studies (see, for example, Ashrafi & Shabani, 2009; Moradi, 2013) deal with nanotori obtained from a C_4C_8 monolayer of atoms. Such a monolayer is represented by a truncated square tiling $\mathbb{S} = (4 \cdot 8^2)$, a Kepler tiling with symmetry group $G = \langle x, y, a, b\rangle$. The group G is a plane crystallographic group of type *p*4*mm*, which is generated by the translations x, y with vectors separated by an angle of $\pi/2$ radians, the fourfold (counterclockwise) rotation a about O, and the reflection b in the axis through O in the direction of x (Fig. 7*a*).

Analogous to a carbon nanotorus, a (m_1, m_2, n_1, n_2) C_4C_8 nanotorus can also be modeled by a tiling $\overline{\mathbb{S}}$ on a round torus defined by a pair of orthogonal vectors $\mathbf{v}_1 = m_1\mathbf{x} + m_2\mathbf{y}$ and $\mathbf{v}_2 = n_1\mathbf{x} + n_2\mathbf{y}$, where $m_1n_1 + m_2n_2 = 0$. Table 6 lists the subgroups L which give rise to models of C_4C_8 nanotori. For each L, we provide the group G^* and the various possible symmetry groups $\overline{G}$ of the corresponding C_4C_8 nanotorus. If we consider a vertex coloring of $\mathbb{S}$, then we obtain a model of a structural analog of a C_4C_8 nanotorus.

As an illustration, let us take the perfect vertex 2-coloring of $\mathbb{S}$ with color-fixing group $K = \langle x^2, xy, a, yb\rangle \cong$ *c2mm* appearing in Fig. 7(*b*). Using $L = \langle x^4, y^6\rangle \leq K$, we obtain a geometric model of a structural analog of a (4, 0, 0, 6) C_4C_8 nanotorus. This analog, shown in Fig. 8, is composed of two types of atoms (96 in all) that occur in the same number. The symmetry group of this analog is $\overline{K} = \langle \sigma_{\mathbf{v}}, \lambda_6\rangle \cong \mathbf{D}_{3\mathbf{d}}$.

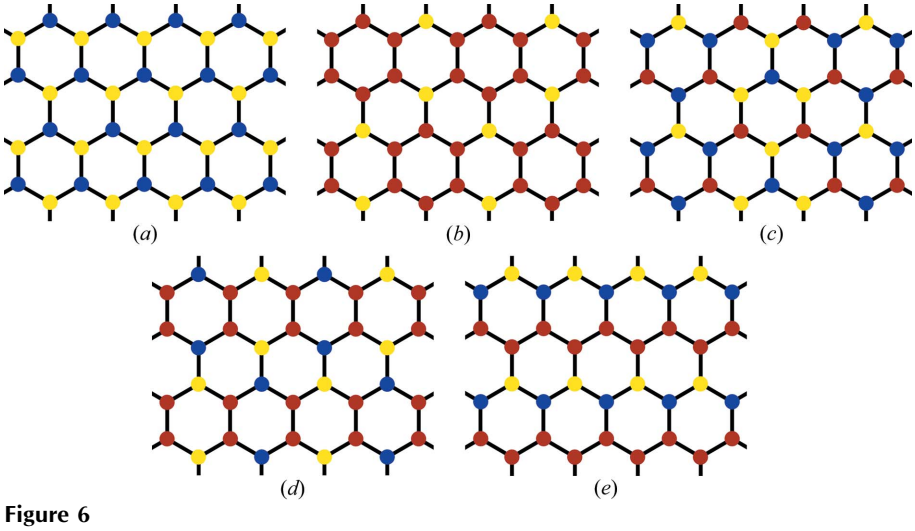

Figure 6
Sections of boron carbon nitride hexagonal monolayers represented by vertex colorings of $\mathbb{H}$. Yellow vertices, boron; red vertices, carbon; blue vertices, nitrogen. (*a*) BN, (*b*) BC_3, (*c*) BCN, (*d*) BC_2N (type I), (*e*) BC_2N (type II).

6. Conclusion and outlook

In this work, we associated two symmetry groups with a tiling $\mathbb{T}^* = \mathbb{T}/L$ on a flat torus $\mathbb{E}^2/L$ obtained as a quotient of a tiling $\mathbb{T}$ of the Euclidean plane $\mathbb{E}^2$: the symmetry group G^* of $\mathbb{T}^*$ itself and the symmetry group $\overline{G}$ of the corresponding tiling $\overline{\mathbb{T}}$ on the round torus.

This paper dealt with the computation and characterization of G^* and $\overline{G}$ when $\mathbb{T}$ is one of the 27 Kepler, Heesch and Laves tilings. We also discussed concepts of color-symmetry theory for these tilings when embedded on a flat torus. One result gives the color group H^* and color-fixing group K^* of a coloring of $\mathbb{T}^*$ in relation to the color group H and color-fixing group K of the corresponding coloring of $\mathbb{T}$, and conversely. A corollary to this result gives a necessary and sufficient condition for a perfect coloring of $\mathbb{T}^*$.

The symmetry group $\overline{G}$ of $\overline{\mathbb{T}}$ was computed by identifying symmetries in G that are transformed into symmetries of $\overline{\mathbb{T}}$. We have determined that $\overline{G}$ arises from one of the seven axial point groups and that its type depends on the position of the pair of vectors used to roll $\mathbb{T}$ into $\overline{\mathbb{T}}$ relative to the centers of rotations and axes of reflections or glide reflections of $\mathbb{T}$ that are in $N_G(L)$.

This paper also demonstrated how a tiling $\overline{\mathbb{T}}$ on a round torus defined by a pair of orthogonal vectors can be employed to model a nanotorus

Table 6
Symmetry groups of C_4C_8 nanotori.

$L = \langle x^{m_1}y^{m_2}, x^{n_1}y^{n_2}\rangle$	$N_G(L)$	G^*	$\overline{G}$
$\lvert m_1\rvert = \lvert m_2\rvert = \lvert n_1\rvert = \lvert n_2\rvert$	$\langle x, y, a, b\rangle \cong p4mm$	$(C_m \times C_{2m}) \rtimes D_4$	$\mathbf{C}_{n\mathbf{v}}$, $\mathbf{D}_{n\mathbf{d}}$, $\mathbf{D}_{n\mathbf{h}}$
$m_2 = 0$, $n_1 = 0$ and $\lvert m_1\rvert = \lvert n_2\rvert$	$\langle x, y, a, b\rangle \cong p4mm$	$(C_m \times C_m) \rtimes D_4$	$\mathbf{C}_{n\mathbf{v}}$, $\mathbf{D}_{n\mathbf{d}}$, $\mathbf{D}_{n\mathbf{h}}$
$\lvert m_1\rvert = \lvert m_2\rvert \neq \lvert n_1\rvert = \lvert n_2\rvert$	$\langle x, y, a^2, ab\rangle \cong cm$	$(C_d \times C_{2mn/d}) \rtimes D_2$	$\mathbf{C}_{n\mathbf{v}}$, $\mathbf{D}_{n\mathbf{d}}$, $\mathbf{D}_{n\mathbf{h}}$
$m_2 = 0$, $n_1 = 0$ and $\lvert m_1\rvert \neq \lvert n_2\rvert$	$\langle x, y, a^2, b\rangle \cong p2mm$	$(C_d \times C_{mn/d}) \rtimes D_2$	$\mathbf{C}_{n\mathbf{v}}$, $\mathbf{D}_{n\mathbf{h}}$
$\lvert m_1\rvert = \lvert n_2\rvert \neq \lvert m_2\rvert = \lvert n_1\rvert$ and $m_2 \neq 0$	$\langle x, y, a\rangle \cong p4$	$(C_d \times C_{(m^2+n^2)/d}) \rtimes C_4$	$\mathbf{C}_{n\mathbf{v}}$, $\mathbf{D}_{n\mathbf{h}}$
Other values	$\langle x, y, a^2\rangle \cong p2$	$(C_d \times C_{\lvert m_1n_2-m_2n_1\rvert/d}) \rtimes C_2$	$\mathbf{C}_{n\mathbf{v}}$, $\mathbf{D}_{n\mathbf{h}}$

$m_1n_1 + m_2n_2 = 0$, $d = \gcd(m_1, m_2, n_1, n_2)$, $m = \gcd(m_1, m_2)$, $n = \gcd(n_1, n_2)$.

obtained from a monolayer of atoms represented by a Kepler tiling $\mathbb{T}$. In particular, we computed the symmetry groups associated with carbon and C_4C_8 nanotori. We have shown that only five types of axial point groups are possible for their symmetry groups. These are $\mathbf{C}_n$, $\mathbf{D}_n$, $\mathbf{C}_{n\mathbf{v}}$, $\mathbf{D}_{n\mathbf{d}}$ and $\mathbf{D}_{n\mathbf{h}}$. We also explained how relevant non-rigid motions of a carbon nanotorus such as whirling motions and torus screw rotations can be identified as motions in G^*.

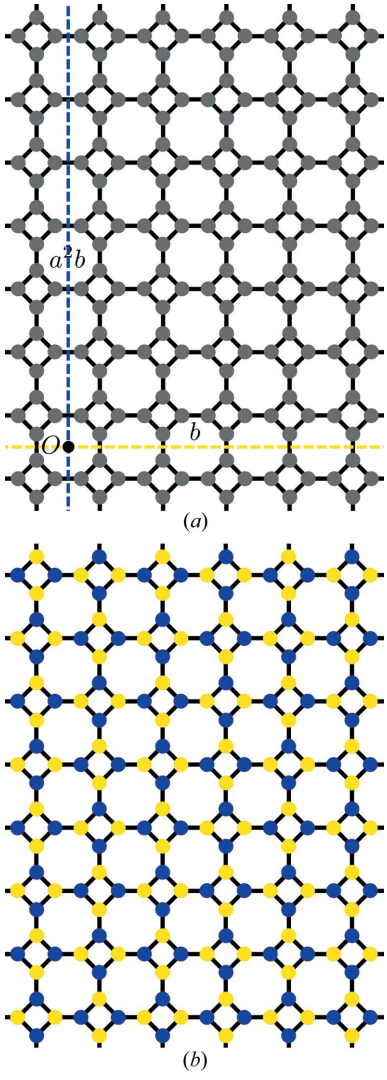

Figure 7
(*a*) An uncolored truncated square tiling $\mathbb{S}$ with axes of reflection of b (yellow) and a^2b (blue). (*b*) A perfect vertex 2-coloring of $\mathbb{S}$.

Vertex colorings of $\overline{\mathbb{T}}$, on the other hand, were employed to model structural analogs of nanotori. The colors in the colored tiling are used to distinguish among different types of atoms. Perfect colorings of $\mathbb{T}^*$ suggest highly symmetric nanotori. An example is the coloring of $\mathbb{H}^*$ obtained from the vertex coloring of $\mathbb{H}$ in Fig. 1(*b*). It was used to model the structural analog in Fig. 5 with an equal distribution of four types of atoms. To illustrate the results highlighted in this work, we computed the symmetry groups associated with structural analogs of carbon nanotori obtained from boron carbon nitride hexagonal monolayers.

This research can be extended to include tilings in the plane without regularity and transitivity properties. Such an extension will cover, for instance, carbon nanotori which contain carbon pentagons and heptagons in addition to carbon hexagons, such as those considered in Beuerle *et al.* (2011) and Chuang *et al.* (2011). One can also consider applying the approach presented in this paper to investigate the symmetry and color-symmetry properties of Kepler, Heesch and Laves tilings embedded on other orbit spaces. It is particularly interesting to see the approach applied to pentaheptite modifications of a graphite sheet (Deza *et al.*, 2000) embedded on Klein bottles and Möbius strips.

APPENDIX *A*

The 11 Kepler tilings, five Heesch tilings and 11 Laves tilings are given in Figs. 9–11, respectively.

The authors would like to acknowledge Ken-ichi Shinoda and Yasushi Gomi of Sophia University, Tokyo, Japan for helpful discussions. GME is grateful to the Accelerated Science and Technology Human Resource Development Program (ASTHRDP) of the Department of Science and Technology (DOST) for her graduate scholarship.

References

Adkins, W. A. & Weintraub, S. H. (1999). *Algebra: an Approach via Module Theory*. New York: Springer-Verlag.

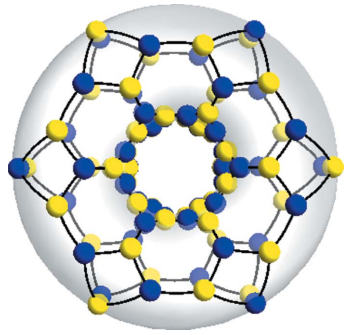

Figure 8
A structural analog of a (4, 0, 0, 6) C_4C_8 nanotorus.

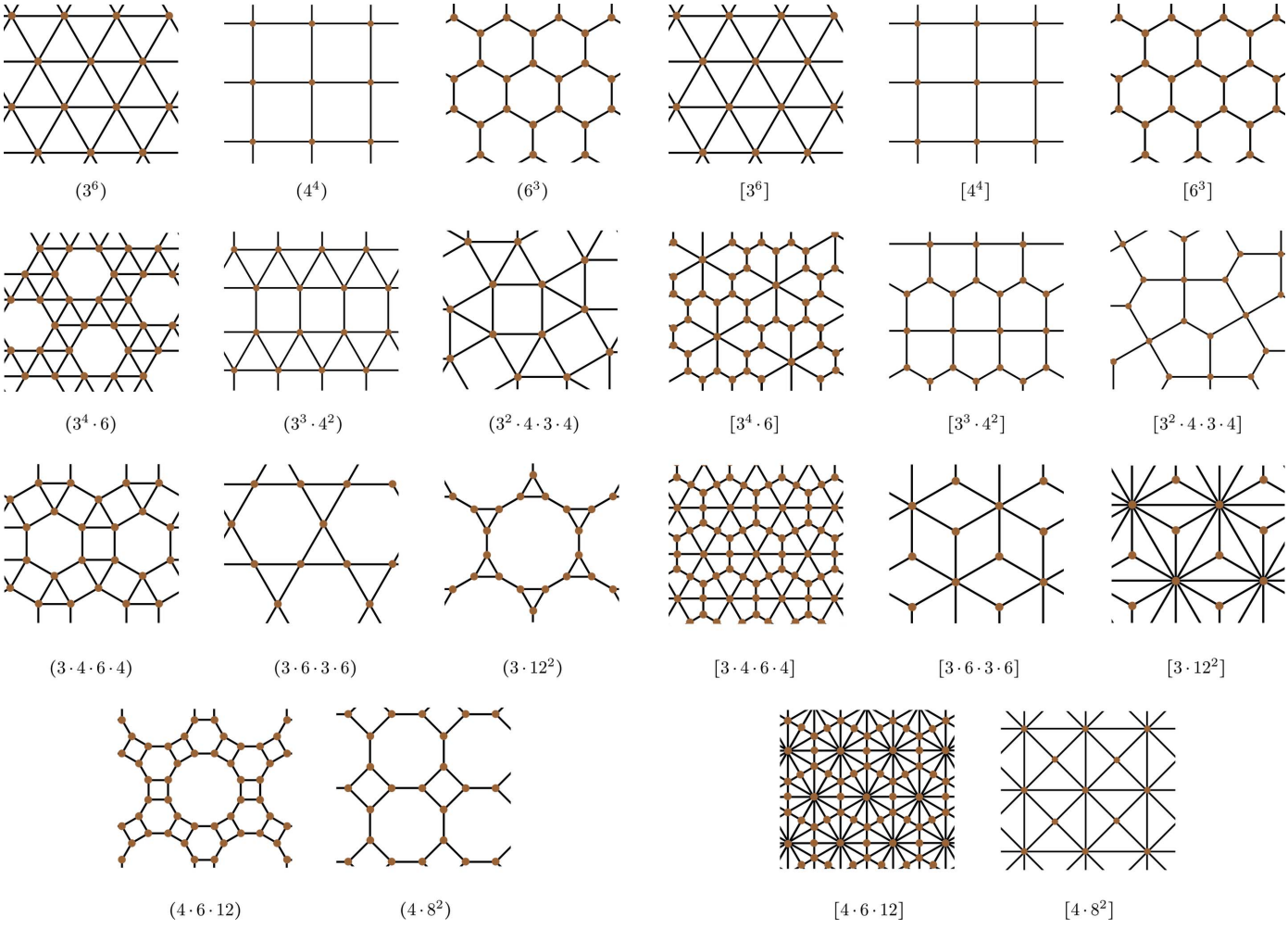

Figure 9
The 11 Kepler tilings.

Figure 11
The 11 Laves tilings.

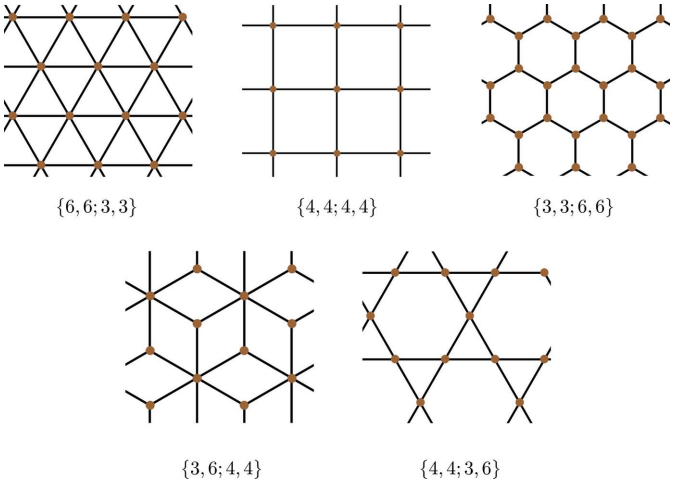

Figure 10
The five Heesch tilings.

Arezoomand, M. & Taeri, B. (2009). *Acta Cryst.* A**65**, 249–252.
Ashrafi, A. R. & Shabani, H. (2009). *Optoelectron. Adv. Mater. Rapid Commun.* **3**, 1309–1314.
Beuerle, F., Herrmann, C., Whalley, A. C., Valente, C., Gamburd, A., Ratner, M. A. & Stoddart, J. F. (2011). *Chem. Eur. J.* **17**, 3868–3875.
Bovin, S. A., Chibotaru, L. F. & Ceulemans, A. (2001). *J. Mol. Catal. A Chem.* **166**, 47–52.
Chuang, C., Fan, Y. C. & Jin, B. Y. (2011). *Procedia Eng.* **14**, 2373–2385.
De Las Peñas, M. L. A. N., Felix, R., Gozo, B. & Laigo, G. (2011). *Philos. Mag.* **91**, 2700–2708.
De Las Peñas, M. L. A. N., Felix, R. P. & Laigo, G. R. (2006). *Z. Kristallogr.* **221**, 665–672.
De Las Peñas, M. L. A. N., Loyola, M. L., Basilio, A. M. & Santoso, E. B. (2014). *Acta Cryst.* A**70**, 12–23.
Deza, M., Fowler, P. W., Shtogrin, M. & Vietze, K. (2000). *J. Chem. Inf. Comput. Sci.* **40**, 1325–1332.
Dienes, K. R. & Thomas, B. (2011). *Phys. Rev. B*, **84**, 085444.
Haddon, R. C. (1997). *Nature (London)*, **388**, 31–32.
Iijima, S. (1991). *Nature (London)*, **354**, 56–58.
Liu, C. P. & Xu, N. (2008). *Physica B*, **403**, 2884–2887.
Liu, L., Jayanthi, C. S. & Wu, S. Y. (2001). *Phys. Rev. B*, **64**, 033412.
Loh, G. C. & Baillargeat, D. (2013). *J. Appl. Phys.* **114**, 183502.
McMullen, P. & Schulte, E. (2002). *Abstract Regular Polytopes*. New York: Cambridge University Press.
Martel, R., Shea, H. R. & Avouris, P. (1999). *Nature (London)*, **398**, 299.
Moradi, S. B.-R. S. (2013). *MATCH Commun. Math. Comput. Chem.* **69**, 165–174.
Oh, D.-H., Park, J. M. & Kim, K. S. (2000). *Phys. Rev. B*, **62**, 1600–1603.

O'Neill, B. (2006). *Elementary Differential Geometry*, 2nd ed. USA: Elsevier.
Sano, M., Kamino, A., Okamura, J. & Shinkai, S. (2001). *Science*, **293**, 1299–1301.
Schattschneider, D. (1978). *Am. Math. Mon.* **85**, 439–450.
Senechal, M. (1988). *Discrete Comput. Geom.* **3**, 55–72.
Sims, C. C. (1994). *Computations with Finitely Presented Groups*. New York: Cambridge University Press.
Staic, M. D. & Petrescu-Nita, A. (2013). *Acta Cryst.* A**69**, 435–439.
Sullivan, J. M. (2011). *Bridges 2011: Mathematics, Music, Art, Architecture, Culture*, pp. 593–596. Phoenix: Tessellations Publishing.
The GAP Group (2013). *GAP – Groups, Algorithms and Programming*, Version 4.7.2. http://www.gap-system.org.
Wolfram Research (2011). *Mathematica Version 8.0 for Microsoft Windows (32-bit)*. http://www.wolfram.com.
Zhao, X., Xing, S., Li, Y., Cai, Z., Pan, Y., Shang, Z., Wang, G., Xu, X. & Li, R. (2012). *J. Math. Chem.* **50**, 2248–2271.